SCIENCE CHINA Materials

ARTICLES

mater.scichina.com link.springer.com

Published online 6 July 2017 | doi: 10.1007/s40843-017-9054-0
Sci China Mater 2017, 60(8): 717–727

Hydrothermal synthesis of coherent porous V_2O_3/carbon nanocomposites for high-performance lithium- and sodium-ion batteries

Xinxin An[1], Hulin Yang[1], Yaping Wang[1], Yan Tang[1], Shuquan Liang[1], Anqiang Pan[1,2*] and Guozhong Cao[3*]

ABSTRACT **Carbonaceous composite materials have been extensively studied in energy storage and conversion devices and commonly are fabricated from liquid precursors. In this work, we reported an unusual formation of vanadium oxide and carbon nanocomposite from microsized VO_2 microspheres through a "dissolution and recrystallization" process with the assistance of LiH_2PO_4. The obtained vanadium oxides nanoparticles are in uniform distribution in the carbon matrix. The V_2O_3/carbon composite inherits the porous feature of the Ketjen black (KB) carbon and has a surface area of 76.59 $m^2 g^{-1}$. As an anode material for lithium/sodium-ion batteries, the V_2O_3/carbon nanocomposites exhibit higher capacity, better rate capability and cycling stability than the V_2O_3 nanoparticle counterparts. The enhanced electrochemical performances are attributed to the porous V_2O_3/carbon nanocomposites, which can allow the electrolyte penetration, shorten the ion diffusion distance and improve the electronic conductivity.**

Keywords: vanadium oxide, porous carbon, lithium-ion batteries, sodium-ion batteries, dissolution and recrystallization

INTRODUCTION

Lithium-ion batteries (LIBs) are used in a wide variety of applications, ranging from portable electronic devices to electric vehicles (EVs) and hybrid electric vehicles (HEVs) because of their high energy density and good stability [1–7]. However, the insufficient storage of lithium resources in the earth, cannot meet the fast growing need [8]. In particular, it is crucially important to explore alternative battery systems for large scale applications [9–11]. Sodium ion batteries (NIBs) have attracted tremendous attention in the past decades due to the abundance storage of sodium resources and the similar chemical reactions for the sodium ions and lithium ions [12–14].

However, NIBs have more requirements for the electrode materials because of the larger Na^+ ions and its slower immigration capability. For example, the commonly used graphite for LIBs can not be used for NIBs because the large Na^+ ions can not intercalate into the layers of graphite [15,16]. Among the potential anode materials for NIBs, transition metal oxides have been explored extensively due to their large capacity. The majority of the transition metals is focused on Fe, Co and Ni based compounds [17–20]. However, much less work has been reported on vanadium based anode materials for NIBs. More recently, V_2O_3 has attracted much attention as anode materials for LIBs due to its low cost, abundant vanadium resources in storage and high theoretical capacity (1070 mA h g^{-1} as lithium battery) [21]. Similar with other transition metal oxides, V_2O_3 also undergoes large volume change during charge/discharge process, which causes the capacity fading for the electrode materials [22–24]. Moreover, the poor electronic conductivity of V_2O_3 also limits its electrochemical properties [25].

Nanostructured electrodes possess lots of advantages, such as unique mechanical, electrical properties and the synergy of bulk and surface properties contributing to the overall behavior [26]. To date, a wide variety of nanostructured materials have been designed and utilized to improve the performance of the energy storage systems [27,28]. Furthermore, in order to solve these obstacles, making vanadium oxides and carbon composites is a common strategy to improve the electrochemical proper-

[1] School of Materials Science and Engineering, Central South University, Changsha 410083, China
[2] State Key Laboratory for Powder Metallurgy, Central South University, Changsha 410083, China
[3] Department of Materials Science & Engineering, University of Washington, Seattle WA 98195, USA
* Corresponding authors (emails: pananqiang@csu.edu.cn (Pan A); gzcao@u.washington.edu (Cao G))

ties. Boukhalfa *et al.* [29] reported the fabrication of atomic layer deposition of vanadium oxide on carbon nanotubes for high-power supercapacitor electrodes and Li *et al.* [30] fabricated carbon fiber cloth@VO_2 composite as an anode for LIBs. For these studies, the vanadium oxides are mainly grown on the conductive carbonaceous materials. However, fabricating coherent porous carbonaceous materials and their usage as anode materials for NIBs are much less studied.

Ketjen black (KB) carbon has been used to make carbonaceous composites due to its low cost, high porosity, easy dispersion and good conductivity [31]. In order to get desired structure, the liquid precursors are commonly employed [32–34]. To date, no research work has been reported on the fabrication of V_2O_3 and KB carbon composite and their electrochemical properties as anode materials for NIBs.

In this work, we reported an unsual formation of coherent V_2O_3 and KB carbon composite from microsized VO_2 microspheres by a facile hydrothermal approach. The VO_2 microspheres are converted into small VO_2 nanoparticles through a dissolution and recrystallization process, distributing homogeneously in the KB carbon matrix. After annealing at high temperature, V_2O_3/carbon nanocomposites with a high porosity can be obtained. As anode materials for LIBs or NIBs, the fabricated V_2O_3 and KB carbon nanocomposites exhibit superior electrochemical properties, which can be attributed to the coherent porous structure of the nanocomposites.

EXPERIMENTAL SECTION

Materials synthesis

The VO_2 microspheres (0.1 g) were prepared according to our previous report [35], which were mixed with LiH_2PO_4(0.188 g), and KB carbon (0.336 g) homogeneously in 30 mL deionized water. Then the mixture solution was sealed in 50-mL PPL-lined stainless steel autoclaves and maintained at 180°C for 12 h. After cooling down to room temperature naturally, the black precipitate was separated by a high-speed centrifuge, washed with absolute alcohol for three times, and then dried at 80°C for 12 h. For comparison, dark blue precipitate was prepared without adding KB carbon in the solvothermal solution while keeping other parameters unchanged. The V_2O_3/carbon nanocomposites and V_2O_3 nanoparticles were obtained by further calcining the obtained precipitates in 5% H_2/95% Ar at 600°C for 4 h with a heating rate of 5°C min^{-1}, respectively.

Materials characterization

The crystallographic phases of both samples were characterized by X-ray diffraction (XRD, Rigaku D/max 2500). The morphologies of samples were examined by scanning electron microscopy (SEM, Quanta FEG 250) and transmission electron microscopy (TEM, JEOL JEM-2100 F). The characteristic of carbon layer was conducted by Raman spectrometer (LabRAM HR800). The thermogravimetric analysis (TGA) was investigated on a combined TG and differential scanning calorimetry (DSC) analysis instrument (Netzsch STA 449C, Germany) from room temperature to 650°C with a heating rate of 10°C min^{-1}. Nitrogen adsorption/desorption isotherms were calculated at 77 K using an adsorption instrument (NOVA4200e, Quantachrome).

Electrochemical measurements

The working anode slurry was prepared by mixing the V_2O_3/carbon nanocomposites, acetylene black and polyvinylidene fluoride (PVDF) binder in *N*-methyl-2-pyrrolidone (NMP) solution with a weight ratio of 80:10:10. The resultant slurry was pasted on copper foil, and was dried in a vacuum oven at 110°C overnight prior to cells assembly. The cells were assembled in an argon-filled glove-box. The electrolyte was 1 mol L^{-1} $LiPF_6$ in ethyl carbonate (EC) and dimethyl carbonate (DMC) (1:1, *v*/*v*) for LIBs. 1 mol L^{-1} $NaClO_4$ in EC and DMC (1:1, *v*/*v*) was used for NIBs. About 50 μL of electrolyte was used per cell. Lithium foil and sodium foil were used as the counter electrodes for LIBs and NIBs, respectively. The galvanostatic charge/discharge experiments were performed using a Land battery tester (Land CT 2001A, China) at room temperature. The mass loading of the active material was about 1 mg cm^{-2}.

RESULTS AND DISCUSSION

Morphology and structure

Scheme 1 illustrates the formation process of V_2O_3/carbon nanocomposites. The VO_2 microspheres and KB carbon were mixed homogeneously in LiH_2PO_4 liquid solution under magnetically stirring until the formation of the slurry. In the followed hydrothermal process, the VO_2 microspheres were converted into small nanoparticles through the dissolution and re-crystallization process with the assistance of LiH_2PO_4. The formed VO_2 nanoparticles were homogeneously distributed within the KB carbon and had good contact between them. After annealing in the mixture gas of 5% H_2/95% Ar at 600°C for 4 h, the VO_2/KB composite can be transformed into V_2O_3 and KB

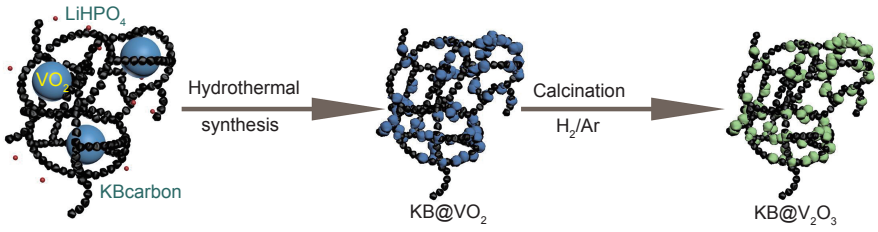

Scheme 1 The illustration of the formation of V_2O_3/carbon nanocomposites.

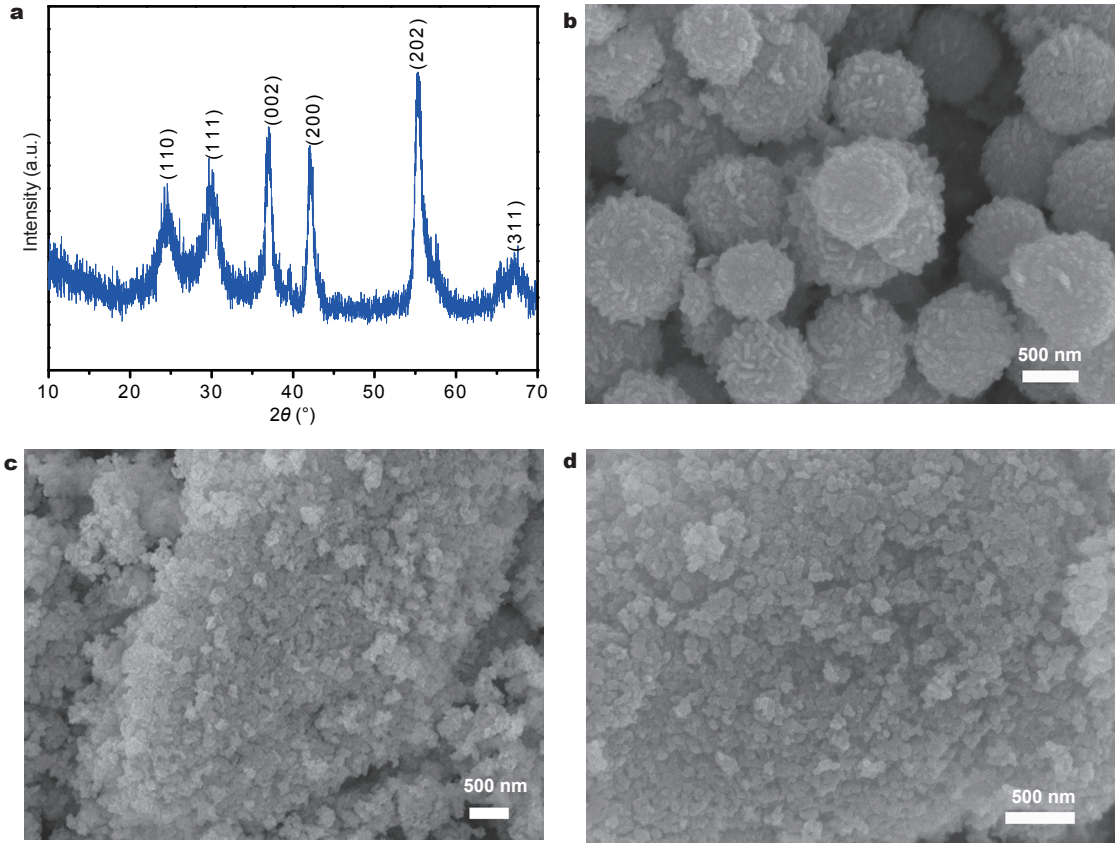

Figure 1 (a) XRD patterns of the precursor of V_2O_3/carbon nanocomposites. SEM images of the vanadium oxide prepared from different hydrothermal solution (b) without and (c) with LiH_2PO_4. (d) SEM images of the precursor of V_2O_3/carbon nanocomposites.

carbon composites, which have good structural reservation from the VO_2/KB composite.

Fig. 1a shows the XRD pattern of the hydrothermal product, which can be assigned to the monoclinic VO_2 phase (a = 4.5968Å, b = 5.6844Å, c = 4.9133Å, β = 89.39°). The result indicates that the hydrothermal treatment does not change the crystallography phase of the VO_2 microspheres. However, the morphologies of the hydrothermal products are in a big difference with or without the addition of LiH_2PO_4 in the hydrothermal solution. As shown in Fig. 1b, the VO_2 microspheres can retain its original morphology when no LiH_2PO_4 was added in the hydrothermal solution. However, the VO_2 microspheres have changed into VO_2 nanoparticles with the addition of LiH_2PO_4 in the hydrothermal solution (see Fig. 1c). The results demonstrate that the existence of LiH_2PO_4 has played a big effect on the structural evolution from VO_2 microspheres to nanoparticles. The structural changes can be explained by a dissolution and recrystallization process. Because of the ionization of LiH_2PO_4, the solution becomes acidic. The VO_2 solid microspheres may dissolve in the above solution under high pressure to form metastable

solution, which is later decomposed to small nanoparticles. During this "dissolution and recrystallization process", the VO_2 phase can be distributed homogeneously into the carbon matrix, thus forming the VO_2 nanoparticles and KB carbon composites (see Fig. 1d).

Fig. 2 shows the structural characterization results of the products after annealing at 600°C for 4 h under the flow of 5% H_2/95% Ar. Fig. 2a shows the XRD patterns of the annealed products from VO_2 nanoparticles and VO_2/KB carbon nanocomposite precursors. All the diffraction peaks can be indexed to the rhombohedral-phase crystalline V_2O_3 (space group: *R*3*c* 167) for both samples. The cell parameters of V_2O_3 in the composite was calculated by Rietveld refinement method (Fig. 2b) and the obtained a = 4.95493 Å and c = 13.98492 Å. The results indicate the VO_2 phase has been converted into V_2O_3 during the high temperature annealing process. The formation of V_2O_3 from VO_2 nanoparticles can be attributed to the reduction of VO_2 by H_2 in the mixed 95% Ar/5% H_2 flowing gas. The phase transformation can be expressed as $2VO_2+H_2 \rightarrow V_2O_3+H_2O$. However, VO_2 nanoparticles may also be reduced to V_2O_3 by carbon at high temperature and the other possible chemical formula of the reaction is $VO_2+C \rightarrow V_2O_3+CO_x$. Interestingly, the width of the XRD peaks for the V_2O_3/KB composite is broader than the V_2O_3 nanoparticles. The difference can be attributed to the smaller crystallites of V_2O_3 in the nanocomposites. Moreover, no carbon related diffraction peak was detected for the V_2O_3/KB carbon nanocomposites, demonstrating the amorphous state or low crystallization of KB carbon in the nanocomposites [21,34]. Fig. 2c displays the SEM image of the V_2O_3 nanoparticles without the addition of KB carbon. The obtained V_2O_3 is consisted of particles with heterogeneous size, some of which exhibit small plate-like morphology and stack together. In general, the particles are in a small size. Fig. 2d shows the SEM image of the as-obtained V_2O_3 and KB carbon nanocomposites. The small plate-like particles can be clearly detected, which is in good consistence with the V_2O_3 particles in Fig. 2c. It is worth noting that the small nanoplates are uniformly surrounded by KB carbon. Moreover, the porous feature of the nanocomposites can be clearly observed. This structure is very important for the penetration of electrolyte. According to the SEM images, the V_2O_3 nanoparticles are more closely stacked and are believed to have a smaller specific surface area than the V_2O_3/KB carbon nanocomposites. Fig. 2e shows the TEM image of the composite, which demonstrates the homogeneous distribution of V_2O_3 in the KB carbon matrix. The V_2O_3 nanoparticles are less than 50 nm and have good contact with the carbon material. Moreover, the porous feature of the nanocomposites is also well revealed, which is mainly inherited from the KB carbon. Fig. 2f shows a high-resolution TEM (HRTEM) image of the nanocomposites, which reveals the V_2O_3 nanoparticles with good planar fringes are in good contact with the KB carbon. Fig. 2f presents elemental mapping images on the V_2O_3/carbon nanocomposites. The C, V and O elements are uniformly distributed in the composites, which suggests the high quality of the V_2O_3 and KB carbon nanocomposites.

In order to get more detailed information about the porosity of the annealed products, nitrogen adsorption-desorption isothermal measurements were carried out for both V_2O_3 nanoparticles and V_2O_3/KB carbon nanocomposites, and the results are shown in Fig. 3. The N_2 adsorption-desorption isotherms (Fig. 3a) can be classified as the type-IV hysteresis loop, indicating the existence of the mesoporous structure [5]. The Brunauer–Emmett–Teller (BET) surface area of the V_2O_3/carbon nanocomposites is 76.59 $m^2 g^{-1}$, which is far more than that of the pure V_2O_3 nanoparticles (27.55 $m^2 g^{-1}$). Fig. 3b displays the Barrette-Joyner-Halenda (BJH) pore-size-distribution plots of the two samples. The main pores in the V_2O_3/carbon nanocomposites are less than 10 nm. The majority of the pores for the V_2O_3 nanoparticles range from 20 to 50 nm. The results suggest the homogenous distribution of V_2O_3 in the KB carbon matrix. Moreover, the small pores in the nanocomposites can be attributed to the KB carbon, which can provide the coherent carbon framework for the electrolyte penetration. The electrode materials with easy electrolyte penetration have been reported in many previous works [31,33].

The Raman spectroscopy of the V_2O_3/carbon nanocomposites (Fig. 4a) shows two characteristic bands of carbonaceous materials located at 1326 cm^{-1} (D-band, disordered carbon) and 1594 cm^{-1} (G-band, graphene carbon), respectively. The result confirms the existence of carbon in the composites. The intensity ratio of the D- and G- bands for the V_2O_3/carbon nanocomposites is I_D/I_G = 1.05, suggesting the existence of the disordered carbon in the composites. However, the small ratio indicates the graphic carbon exists in a large portion, which would be helpful for improving the electronic conductivity of the V_2O_3/carbon nanocomposites [31].

Fig. 4b shows the TGA result of V_2O_3/carbon nanocomposites, which was conducted in air ranging from room temperature to 650°C using a heating rate of 10°C min^{-1}. The initial weight loss before 150°C can be attributed to the evaporation of the physical or chemical bonded water in the composites. The followed weight increase can

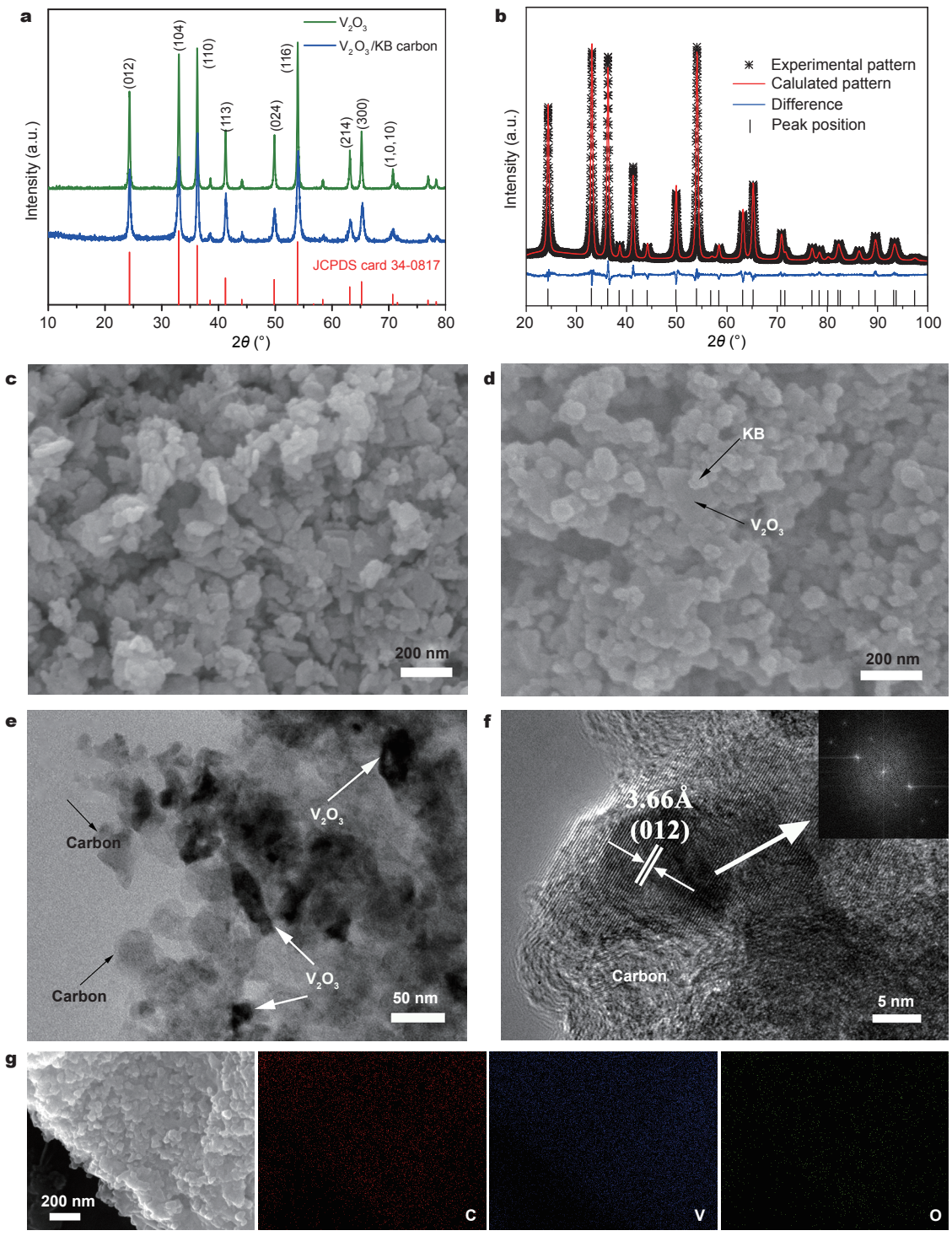

Figure 2 (a) XRD patterns of the V_2O_3/carbon nanocomposites and the pure V_2O_3 nanoparticles. (b) XRD pattern with Rietveld refinement of the V_2O_3/carbon nanocomposites. (c) SEM of the pure V_2O_3 nanoparticles. (d) SEM of the V_2O_3/carbon nanocomposites. (e) TEM, (f) HRTEM and (g) STEM-high-angle annular dark field (HAADF) image and energy disperse spectroscopy (EDS) elemental mapping images of V_2O_3/carbon nanocomposites.

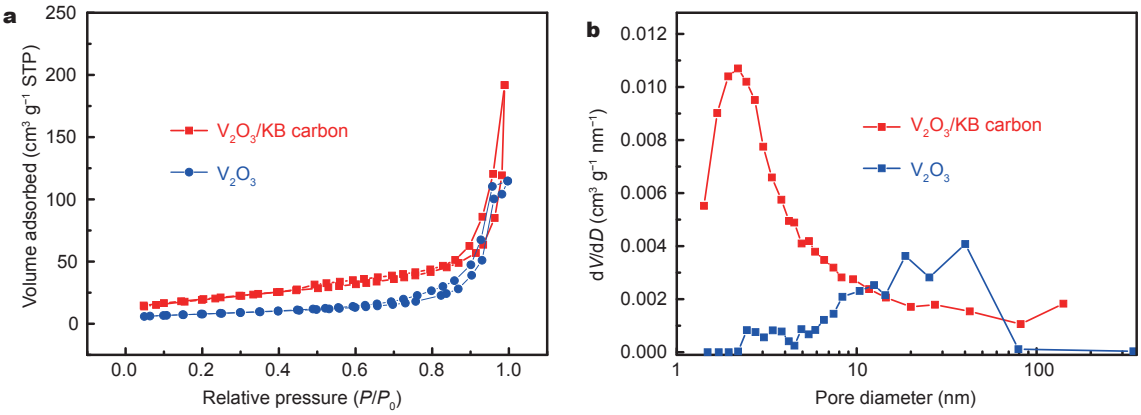

Figure 3 (a) Nitrogen adsorption/desorption isotherms and (b) pore size distribution of the V_2O_3/carbon nanocomposites and V_2O_3 nanoparticles.

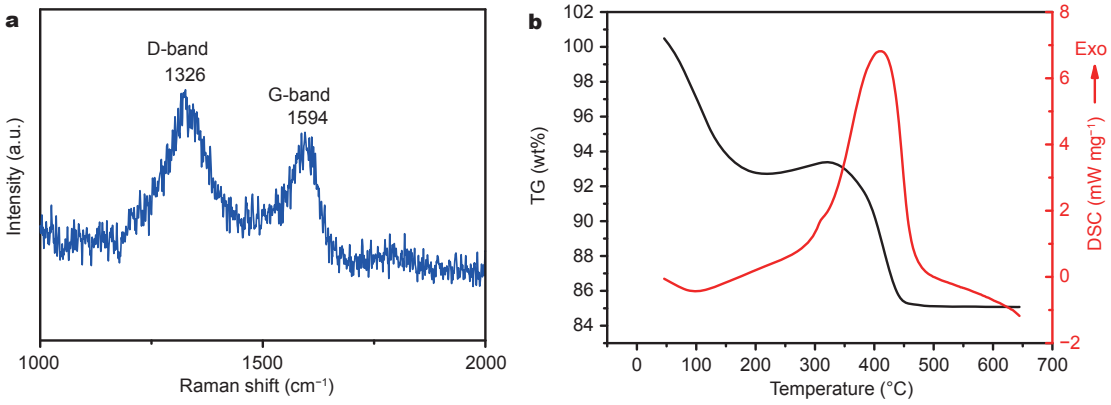

Figure 4 (a) Raman spectrum of the V_2O_3/carbon nanocomposites. (b) TG and DSC curves of the V_2O_3/carbon nanocomposites.

be attributed to the oxidation of V_2O_3 to V_2O_5 in the air. At elevated temperature, the weight loss can be assigned to the combustion of KB carbon. It is believed the oxidation of vanadium oxides and the combustion of KB carbon happen simultaneously between 300 and 450°C. The weight becomes constant after 500°C due to their complete conversion into V_2O_5. According to the TGA result, the weight percentage of the V_2O_3 particles in the V_2O_3/carbon nanocomposites is 75.63 wt.%.

Lithium-ion battery performance

Fig. 5 displays the electrochemical performances of the V_2O_3 and KB carbon nanocomposites as cathode materials for LIBs. Fig. 5a shows the cycling performance of the composites electrode at the current density of 100 mA g^{-1}, which delivers an initial specific discharge capacity of 1140 mA h g^{-1} and retains a stable capacity of 587 mA h g^{-1} after 200 cycles. The initial capacity fading can be attributed to the irreversible capacity contribution from the electrolyte decomposition to form the solid electrolyte interphase layer between the electrode and electrolyte. For comparison, the V_2O_3 nanoparticles electrode only deliver a stable capacity of 192 mAh g^{-1} and the KB carbon only has a stable capacity of 284 mA h g^{-1}. The result demonstrates that the electrochemical performance has been greatly improved by preparing the V_2O_3 and KB carbon nanocomposites. Fig. 5b shows the discharge/charge curves of the selected cycles for the composites. The shape of the curves is quite similar, which demonstrates its good structural reversibility for the V_2O_3 and KB carbon nanocomposites. Fig. 5c shows the rate performance of the composites and V_2O_3 nanoparticles electrodes. The composite electrodes exhibit the specific capacities of 774.8, 589.8, 545.3, 471.7, 325.2and 219.1 mA h g^{-1} at the current densities of 100, 200, 300, 500, 1000 and 2000 mA g^{-1}, respectively. The electrode materials were retested for another round and similar rate performance can be achieved for the composites electrodes. When the current was reset to 100 mA g^{-1}, a stable capacity of 713 mA h g^{-1} can be obtained. The capacity is higher than the initial

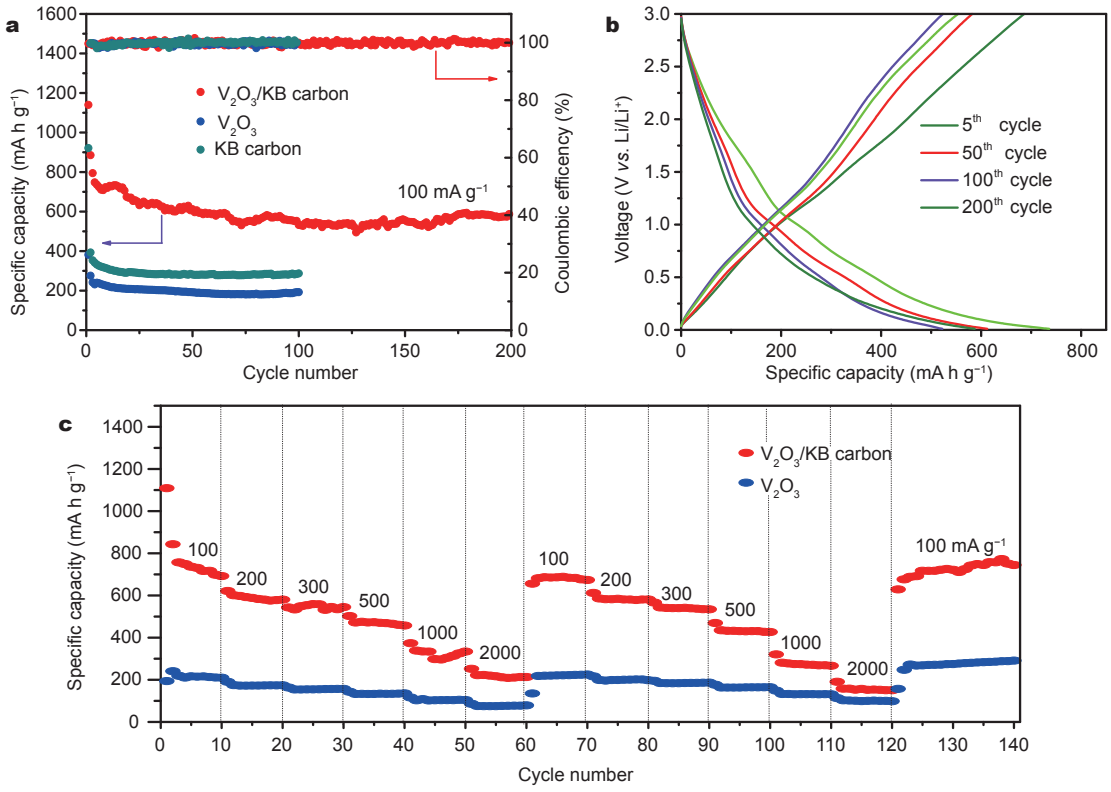

Figure 5 Electrochemical lithium storage performance of the V_2O_3/carbon nanocomposites, pure V_2O_3 particles and KB carbon in the window of 0.01–3V (*vs.* Li/Li^+). (a) Cycling performance of the three electrode materials at a current density of 100 mA g^{-1}. (b) Galvanostatic discharge/charge curves for the 5th, 10th, 50th, 100th and 200th cycles at 100 mA g^{-1}. (c) Rate performance of the V_2O_3/carbon nanocomposites and pure V_2O_3 particles.

capacity delivered at 100 mA g^{-1}, which can be attributed to the improved wettability of the composites electrode materials after repeated cycles. Moreover, the rate performance is much better than the V_2O_3 nanoparticles electrode. The superior electrochemical performances, including higher capacity and better rate capability, can be ascribed to the coherent V_2O_3 and KB carbon composites. According to the SEM and TEM results, the V_2O_3 and KB carbon nanocomposites are of high porosity, which can provide the easy electrolyte penetration ways and increase the contact area between the electrode materials and electrolyte. Moreover, the good contact between V_2O_3 and KB carbon can improve the electronic conductivity of the nanocomposites.

Sodium-ion battery performance

The electrochemical performances of the V_2O_3/carbon nanocomposites, KB carbon and V_2O_3 nanoparticles as cathode materials for NIBs are shown in Fig. 6. Fig. 6a shows the cycling performance of the three electrode materials at the current density of 100 mA g^{-1}, suggesting that the discharge capacity of the V_2O_3/carbon nanocomposites, pure KB carbon and V_2O_3 nanoparticles on the 1st cycle are 744.6, 879.6 and 281 mA h g^{-1}, respectively. After 150 cycles, the three electrodes deliver the specific discharge capacity of 270, 100 and 98 mA h g^{-1}, respectively. The results indicate the improved sodium storage capability for the V_2O_3 and KB carbon composites. Moreover, the capacity of the V_2O_3 and KB carbon composites is quite stable after the initial five cycles. Therefore, the V_2O_3/KB composite electrode also exhibits more excellent cycle stability than other vanadium oxide used as sodium storage material [36]. Fig. 6b shows the charge/discharge profiles of the V_2O_3/carbon nanocomposites at a current density of 100 mA g^{-1}. As can be seen in the picture, the charge/discharge curves for the 2nd, 5th, 10th, 50th and 100th cycles coincide with each other, suggesting remarkable cycle stability. The rate capability was tested by gradually growing current densities from 100 to 1000 mA g^{-1}. As shown in the Fig. 6c, even after a second round rate capability measurement, the electrode can also exhibit a high specific discharge capacity of 270.8 mA h g^{-1} when

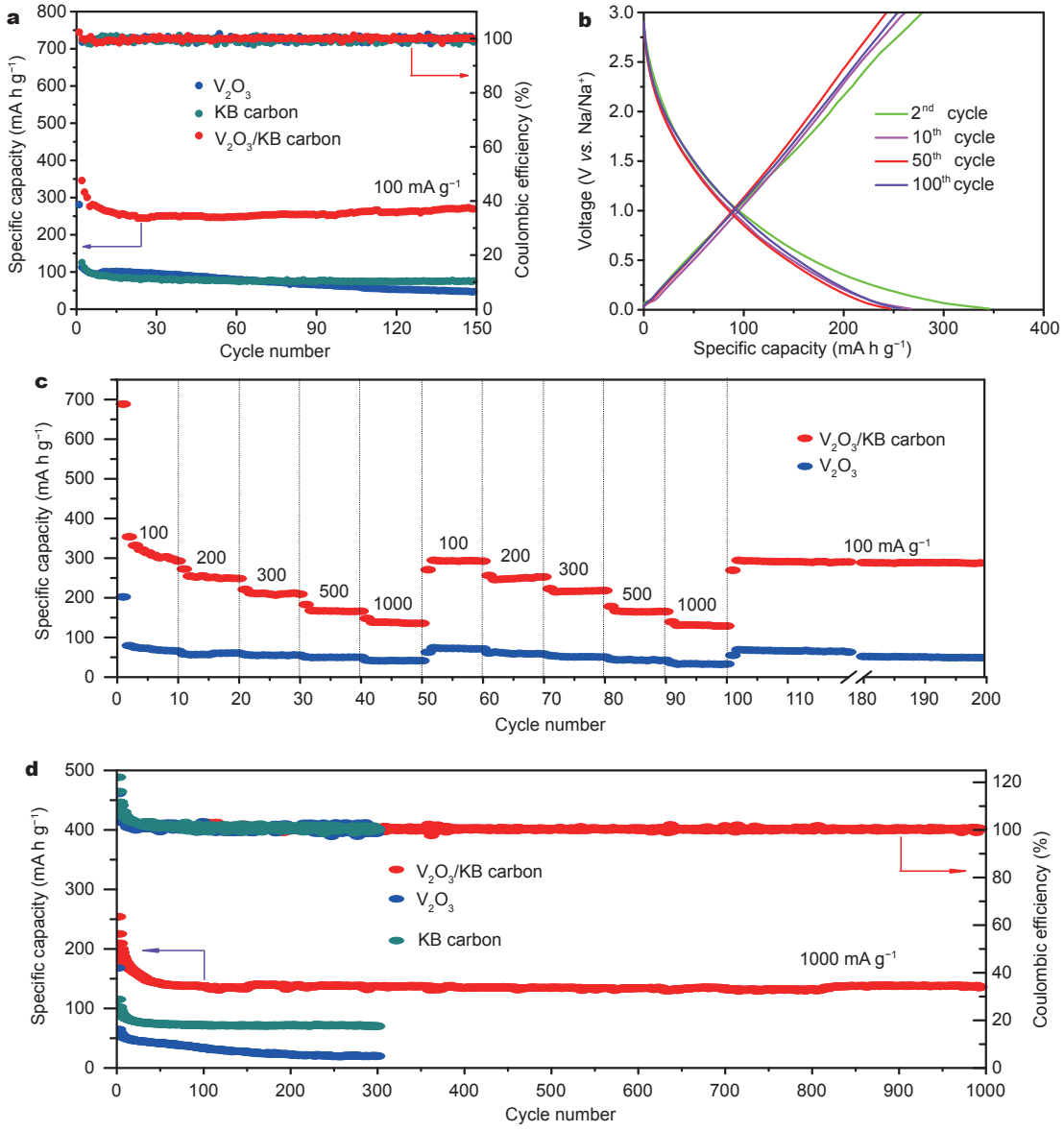

Figure 6 Electrochemical sodium storage performance of the V_2O_3/carbon nanocomposites, V_2O_3 particles and KB carbon in the voltage range of 0.01–3 V (*vs.* Na/Na$^+$). (a) Cycling performance at a current density of 100 mA g^{-1}. (b) Galvanostatic discharge/charge curves for the 2nd, 5th, 10th, 50th and 100th cycles at 100 mA g^{-1}. (c) Rate performance of the two electrode materials. (d) Cycling performance at a current density of 1000 mA g^{-1}.

the current density returned to 100 mA g^{-1}. However, the pure V_2O_3 nanoparticles electrode can only deliver 62.9 mA h g^{-1}. The result demonstrates the V_2O_3/carbon nanocomposite electrodes have good rate performance as sodium electrode material. Fig. 6d shows the cycling performance of the three electrodes at a current density of 1000 mA g^{-1}. The initial specific discharge capacity of the V_2O_3/carbon nanocomposites (444.8 mA h g^{-1}) is much higher than 168 mA h g^{-1} for the V_2O_3 nanoparticles and 165 mA h g^{-1} for the pure KB carbon. Moreover, the capacity of the V_2O_3/carbon nanocomposites is quite stable over 1000 cycles. However, the discharge capacity of the V_2O_3 nanoparticles presents an obvious decline over 300 cycles. Although the discharge capacity of the pure KB carbon is stable, the discharge capacity is approximately 50% of the capacity for the V_2O_3/carbon nanocomposites.

Electrochemical impedance spectroscopy (EIS) measurement was conducted to better explore the reason for the improved electrochemical performance of the V_2O_3/carbon composite. Fig.7 shows the obtained results and its

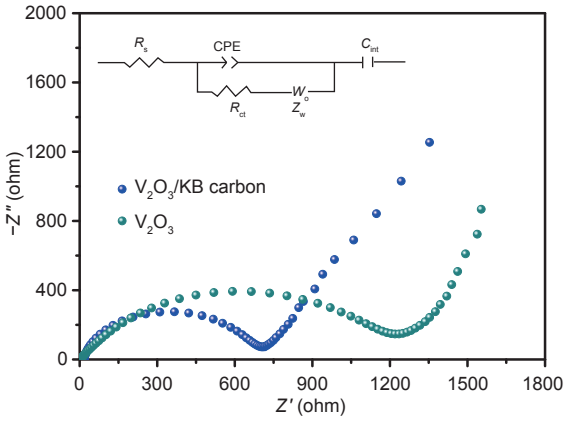

Figure 7 Nyquist plots of the V_2O_3 and V_2O_3/carbon nanocomposites as anodes for NIBs and their simulation model for the calculation.

used equivalent circuit, in which R_s represents the combination of electrolyte resistance and Ohmic resistances of cell components. R_{ct} and CPE stand for charge transfer resistance between the electrode and the electrolyte and double layer capacitance on the electrode surface, respectively. As anode for NIBs, the simulated charge transfer resistance (R_{ct}) of the V_2O_3/carbon nanocomposite is 639.5 Ω, which is much smaller than 1233.1 Ω for the pure V_2O_3 electrode. The improvement can be mainly attributed to the coherent porous V_2O_3/carbon nanocomposites framework and the good contact between V_2O_3 and KB carbon, which facilitate the electrolyte penetration and improve the electronic conductivity of the nanocomposites.

According to the electrochemical performances mentioned above, the V_2O_3/carbon composite electrodes exhibit higher specific capacities, better rate capability and cyclic stability. The enhanced sodium storage capability for the composite electrodes can be attributed to the coherent porous structures. The KB carbon can improve the electronic conductivity of the electrode materials and the coherent porous structure can facilitate the electrolyte penetration and enlarge the contact area between electrode and electrolyte, which can result in higher capacity and better rate capability. Moreover, the vanadium oxide in the composite can keep better integrity during the repeated cycles, thus exhibiting improved cycling stability.

CONCLUSIONS

In summary, the coherent V_2O_3/carbon nanocomposites has been synthesized *via* a facile hydrothermal method and a followed annealing process. The VO_2 microspheres are converted into VO_2 nanoparticles *via* a dissolution and recrystallization process, and distribute homogeneously in the KB carbon matrix. The obtained V_2O_3 and KB carbon nanocomposites are of high porosity and have a surface area of 76.59 $m^2 g^{-1}$. As cathode materials for LIB or NIBs, the composite electrode materials exhibit high capacity, good rate capability and cycling stability. The good electrochemical performances are attributed to the V_2O_3/carbon nanocomposites which possess high electronic conductivity, large specific surface area, and high porosity.

Received 31 March 2017; accepted 23 May 2017; published online 6 July 2017

1 Tarascon JM, Poizot P, Laruelle S, *et al.* Nano-sized transition-metal oxides as negative-electrode materials for lithium-ion batteries.. Nature, 2000, 407: 496–499
2 Wang DW, Li F, Liu M, *et al.* 3D aperiodic hierarchical porous graphitic carbon material for high-rate electrochemical capacitive energy storage. Angew Chem, 2008, 120: 379–382
3 Yang S, Gong Y, Liu Z, *et al.* Bottom-up approach toward single-crystalline VO_2-graphene ribbons as cathodes for ultrafast lithium storage. Nano Lett, 2013, 13: 1596–1601
4 Zhang P, Zhao L, An Q, *et al.* A high-rate V_2O_5 hollow microclew cathode for an all-vanadium-based lithium-ion full cell. Small, 2016, 12: 1082–1090
5 Wang L, Bi X, Yang S. Partially single-crystalline mesoporous Nb_2O_5 nanosheets in between graphene for ultrafast sodium storage. Adv Mater, 2016, 28: 7672–7679
6 Wang H, Zhang X. Designing multi-shelled metal oxides: towards high energy-density lithium-ion batteries. Sci China Mater, 2016, 59: 521–522
7 Zeng L, Pan A, Liang S, *et al.* Novel synthesis of V_2O_5 hollow microspheres for lithium ion batteries. Sci China Mater, 2016, 59: 567–573
8 Uchaker E, Zheng YZ, Li S, *et al.* Better than crystalline: amorphous vanadium oxide for sodium-ion batteries. J Mater Chem A, 2014, 2: 18208–18214
9 Fu B, Zhou X, Wang Y. High-rate performance electrospun $Na_{0.44}MnO_2$ nanofibers as cathode material for sodium-ion batteries. J Power Sources, 2016, 310: 102–108
10 Sun W, Rui X, Zhang D, *et al.* Bismuth sulfide: a high-capacity anode for sodium-ion batteries. J Power Sources, 2016, 309: 135–140
11 Yin L, Wang Y, Han C, *et al.* Self-assembly of disordered hard carbon/graphene hybrid for sodium-ion batteries. J Power Sources, 2016, 305: 156–160
12 Ali G, Lee JH, Oh SH, *et al.* Investigation of the Na intercalation mechanism into nanosized V_2O_5/C composite cathode material for Na-ion batteries. ACS Appl Mater Interfaces, 2016, 8: 6032–6039
13 Hong SY, Kim Y, Park Y, *et al.* Charge carriers in rechargeable batteries: Na ions *vs.* Li ions. Energ Environ Sci, 2013, 6: 2067–2081
14 Wang X, Niu C, Meng J, *et al.* Novel $K_3V_2(PO_4)_3$/C bundled nanowires as superior sodium-ion battery electrode with ultrahigh cycling stability. Adv Energ Mater, 2015, 5: 1500716
15 Yabuuchi N, Kubota K, Dahbi M, *et al.* Research development on sodium-ion batteries. Chem Rev, 2014, 114: 11636–11682
16 Kim H, Kim H, Ding Z, *et al.* Recent progress in electrode materials for sodium-ion batteries. Adv Energ Mater, 2016, 6: 1600943

17 Jiang Y, Hu M, Zhang D, *et al.* Transition metal oxides for high performance sodium ion battery anodes. Nano Energ, 2014, 5: 60–66
18 Deng Q, Wang L, Li J. Electrochemical characterization of Co_3O_4/MCNTs composite anode materials for sodium-ion batteries. J Mater Sci, 2015, 50: 4142–4148
19 Jian Z, Zhao B, Liu P, *et al.* Fe_2O_3 nanocrystals anchored onto graphene nanosheets as the anode material for low-cost sodium-ion batteries. Chem Commun, 2014, 50: 1215–1217
20 Nie Z, Wang Y, Zhang Y, *et al.* Multi-shelled α-Fe_2O_3 microspheres for high-rate supercapacitors. Sci China Mater, 2016, 59: 247–253
21 Shi Y, Zhang ZJ, Wexler D, *et al.* Facile synthesis of porous V_2O_3/C composites as lithium storage material with enhanced capacity and good rate capability. J Power Sources, 2015, 275: 392–398
22 Jiang L, Qu Y, Ren Z, *et al. In situ* carbon-coated yolk–shell V_2O_3 microspheres for lithium-ion batteries. ACS Appl Mater Interfaces, 2015, 7: 1595–1601
23 Sun Y, Jiang S, Bi W, *et al.* Highly ordered lamellar V_2O_3-based hybrid nanorods towards superior aqueous lithium-ion battery performance. J Power Sources, 2011, 196: 8644–8650
24 Niu C, Huang M, Wang P, *et al.* Carbon-supported and nanosheet-assembled vanadium oxide microspheres for stable lithium-ion battery anodes. Nano Res, 2016, 9: 128–138
25 Wang Y, Zhang HJ, Admar AS, *et al.* Improved cyclability of lithium-ion battery anode using encapsulated V_2O_3 nanostructures in well-graphitized carbon fiber. RSC Adv, 2012, 2: 5748–5753
26 Wang L, Hu Z, Zhao K, *et al.* Hollow spherical $LiNi_{0.5}Mn_{1.5}O_4$ built from polyhedra with high-rate performance *via* carbon nanotube modification. Sci China Mater, 2016, 59: 95–103
27 Zhang X, Cheng X, Zhang Q. Nanostructured energy materials for electrochemical energy conversion and storage: a review. J Energ Chem, 2016, 25: 967–984
28 Wei Q, Xiong F, Tan S, *et al.* Porous one-dimensional nanomaterials: design, fabrication and applications in electrochemical energy storage. Adv Mater, 2017, 29: 1602300
29 Boukhalfa S, Evanoff K, Yushin G. Atomic layer deposition of vanadium oxide on carbon nanotubes for high-power supercapacitor electrodes. Energ Environ Sci, 2012, 5: 6872
30 Li S, Liu G, Liu J, *et al.* Carbon fiber cloth@VO_2 (B): excellent binder-free flexible electrodes with ultrahigh mass-loading. J Mater Chem A, 2016, 4: 6426–6432
31 Pan A, Liu J, Zhang JG, *et al.* Nano-structured $Li_3V_2(PO_4)_3$/carbon composite for high-rate lithium-ion batteries. Electrochemistry Commun, 2010, 12: 1674–1677
32 Su Y, Pan A, Wang Y, *et al.* Template-assisted formation of porous vanadium oxide as high performance cathode materials for lithium ion batteries. J Power Sources, 2015, 295: 254–258
33 Dong H, Xu Y, Ji M, *et al.* High performance of mesoporous γ-Fe_2O_3 nanoparticle/Ketjen black composite as anode material for lithium ion batteries. Electrochim Acta, 2015, 151: 118–125
34 Zhang Y, Dong H, Zhang H, *et al.* $Li_4Ti_5O_{12}$/Ketjen black with open conductive frameworks for high-performance lithium-ion batteries. Electrochim Acta, 2016, 201: 179–186
35 Pan A, Wu HB, Yu L, *et al.* Template-free synthesis of VO_2 hollow microspheres with various interiors and their conversion into V_2O_5 for lithium-ion batteries. Angew Chem, 2013, 125: 2282–2286
36 He G, Li L, Manthiram A. VO_2 /rGO nanorods as a potential anode for sodium- and lithium-ion batteries. J Mater Chem A, 2015, 3: 14750–14758

Acknowledgements This work was supported by the National Natural Science Foundation of China (51302323), the Program for New Century Excellent Talents in the University (NCET-13-0594), the Research Fund for Doctoral Program of Higher Education of China (201301621200), and the Natural Science Foundation of Hunan Province, China (14JJ3018).

Author contributions An X and Wang Y participated in the experiment and wrote the article. Yang H participated in the experiment and drew the scheme and figures. Pan A and Cao G conceived and supervised the project and revised the manuscript. All authors contributed to the general discussion.

Conflict of interset The authors declare that they have no conflict of interest.

Xinxin An is a postgraduate student in Prof. Pan's Group and will receive her MSc degree from the School of Materials Science and Engineering, Central South University in June 2017. Her current research interest is the vanadium-based electrode material for lithium ion battery.

Hulin Yang is a postgraduate student in Prof. Pan's Group will receive his MSc degree from the School of Materials Science and Engineering, Central South University in 2018. His current research interest is the tin sulfide hollow microsphere for anode of lithium ion battery.

Anqiang Pan received his PhD degree (2011) from Central South University. He joined Prof. Guozhong Cao's group at the University of Washington as a visiting student in 2008. Then, he worked at PNNL as a visiting scholar in Drs. Ji-Guang Zhang and Jun Liu's group (2009–2011). He joined Prof. Xiongwen (David) Lou's group at Nanyang Technological University as a research fellow (2011-2012). Currently, he is a Sheng-Hua Professor at Central South University. His current interests are on the lithium/sodium ion batteries, and supercapacitors.

水热法制备多孔V_2O_3/碳复合材料用于高性能锂离子电池和钠离子电池的研究

安欣欣[1], 杨岵林[1], 王亚平[1], 唐艳[1], 梁叔全[1], 潘安强[1,2*], 曹国忠[3*]

摘要 碳复合材料已经在能量储存和转换设备中得到广泛的研究, 并且通常由液体前驱体制备. 本文报道了在LiH_2PO_4的帮助下, VO_2微米球通过“溶解和重结晶”, 形成V_2O_3和碳纳米复合材料的特殊过程. 得到的钒氧化物纳米颗粒在碳基体中分布均匀. V_2O_3/碳复合材料继承了KB碳的多孔特征, 比表面积为76.59 m^2g^{-1}. 作为锂/钠离子电池的负极材料, V_2O_3/碳复合材料表现出比V_2O_3纳米颗粒更高的放电比容量, 更好的倍率性能和循环稳定性. 电化学性能提高归因于V_2O_3/碳纳米复合材料的多孔结构, 其允许电解质渗透, 缩短离子扩散距离并提高电子导电率.